HHS Public Access

Author manuscript

J Immunol. Author manuscript; available in PMC 2022 May 01.

Published in final edited form as:

J Immunol. 2021 May 01; 206(9): 2135–2145. doi:10.4049/jimmunol.2000899.

Novel mouse model reveals that serine phosphorylation of L-plastin is essential for effective splenic clearance of pneumococcus

Edgar P. Anaya[*], **Xue Lin**[*], **Elizabeth M. Todd**[*], **Taylor P. Szasz**[*], **S. Celeste Morley**[*,#]

[*]Department of Pediatrics, Division of Infectious Diseases, Washington University School of Medicine, St. Louis, MO 63110

[#]Department of Pathology and Immunology, Division of Immunobiology, Washington University School of Medicine, St. Louis, MO 63110

Abstract

Asplenia imparts susceptibility to life-threatening sepsis with encapsulated bacteria, such as the pneumococcus. However, the cellular components within the splenic environment that guard against pneumococcal bacteremia have not been defined. The actin-bundling protein L-plastin (LPL) is essential for generation of marginal zone B cells and for anti-pneumococcal host defense, as revealed by a mouse model of genetic LPL deficiency. In independent studies, serine phosphorylation of LPL at residue 5 (S5) has been described as a key “switch” in regulating LPL actin-binding and subsequent cell motility, although much of the data are correlative. To test the importance of S5 phosphorylation in LPL function, and to specifically assess the requirement of LPL S5 phosphorylation in anti-pneumococcal host defense, we generated the “S5A” mouse – expressing endogenous LPL bearing a serine-to-alanine mutation at this position. S5A mice were bred to homozygosity and LPL was expressed at levels equivalent to WT, but S5 phosphorylation was absent. S5A mice exhibited specific impairment in clearance of pneumococci following intravenous challenge, with 10-fold higher bacterial bloodstream burden 24 h after challenge compared to WT or fully LPL-deficient animals. Defective bloodstream clearance correlated with diminished population of marginal zone macrophages and with reduced phagocytic capacity of multiple innate immune cells. Development and function of other tested leukocyte lineages were normal in S5A mice, such as T and B cell motility and activation. The S5A mouse thus provides a novel system in which to elucidate the precise molecular control of critical immune cell functions in specific host:pathogen defense interactions.

Correspondence to: S. Celeste Morley, Campus Box 8208, 660 S. Euclid Ave., St. Louis, MO, 63110, (t) 314-286-2136 (f) 314-286-2895, morleys@wustl.edu.

Authorship

Conceptualization: E.A., E.M.T., X.L., … S.C.M. Methodology: E.A., E.M.T. X.L,,… and S.C.M. Investigation: E.A., T.S., X. L., E.M.T… Writing – original draft: S.C.M. Writing – review & editing: E.A., X. L., E.M.T. and S.C.M. Funding Acquisition: S.C.M. Supervision: S.C.M.

Introduction

Infection with *Streptococcus pneumoniae* (pneumococcus) remains a major cause of global morbidity and mortality (1). Despite advances in vaccinology, antibiotic developments, and critical care, up to 10% of patients presenting to medical care with pneumococcal sepsis will die. Pneumococcal bacteremia and sepsis pose especially significant risks to asplenic patients, who exhibit 50–70% chance of mortality with pneumococcal bacteremia (2, 3). While the requirement for the spleen in clearing the blood of polysaccharide-encapsulated bacteria, such as pneumococcus, has been well established, the precise cellular and molecular requirements enabling this unique function are not fully elucidated. Splenic tissue is classified into red pulp, through which the blood circulates, and white pulp, discrete collections of lymphoid tissue (follicles) comprised largely of T and B cells. The areas where red and white pulp merge is termed the “marginal zone” (MZ). Innate and adaptive immune cell lineages essential to pneumococcal clearance reside in this borderland. These spleen-specific lineages include marginal zone macrophages (MZM), marginal zone B cells (MZB), and metallophilic macrophages (MMM) (4).

L-plastin (LPL), one of three plastin isoforms, is an actin-bundling protein critical for leukocyte motility (5), and through this role, supports both MZB development and alveolar macrophage (AM) development in the lung (6–8). Mice genetically deficient for LPL (LPL $^{-/-}$) are also highly susceptible to pneumococcal infection (7, 9). By promoting development of alveolar macrophages and MZB, both of which play key roles in anti-pneumococcal defense, LPL illustrates how a molecule often classed as a “structural” protein can serve essential immune functions. However, little is known about the molecular regulatory elements controlling LPL in macrophages and lymphocytes. The regulatory domain of LPL, the sole plastin expressed in leukocytes, is distinguished from the other two plastin isoforms (I- and T-plastin) by two serine phosphorylation sites, at serine 5 (S5) and serine 7 (S7). *In vivo*, LPL S5 is heavily phosphorylated in response to multiple extracellular stimuli, and it was reported in 2006 that S5 phosphorylation increased actin binding and bundling by LPL and enhanced the localization of LPL to actin-rich regions (10). Furthermore, expression of LPL that was phosphorylatable at S5 (wild-type LPL) in 293HEKT enhanced cell migration, while the non-phosphorylatable form of LPL, in which the serine at position 5 was converted to an alanine, did not (10). These data have been highly cited and interpreted to mean that S5A LPL is “inactive” (11).

Since then, many publications have correlated cell activation or migration with LPL S5 phosphorylation (5). For instance, S5 phosphorylation in T cells has been correlated with impaired upregulation of CD69 and CD25 following co-stimulation in T cell activation (12), and immunosuppression of T cell activation by the corticosteroid dexamethasone also correlated with reduced S5 phosphorylation (13). Additionally, S5 phosphorylation has been correlated with homing of B-cell derived chronic lymphocytic leukemia to the bone marrow niche (14), impaired T cell synapse formation and T cell activation (15), and cancer metastasis (16). However, the singular importance of S5 phosphorylation has been challenged by the observation that peptidomimetic inhibition of LPL S5 phosphorylation only modestly impaired LPL-dependent phenotypes osteoclasts (17). Furthermore, highly detailed *in vitro* analysis of the LPL N-regulatory domain found no effect of S5A mutation

on the actin-binding or actin-bundling activity of LPL (18). To resolve prior and current reports, and to establish a new system to elucidate the mechanism by which ablated S5 phosphorylation alters the function of LPL within primary cells, we generated “S5A” mice using CRISPR technology. These mice express the endogenous, full-length LPL locus encoding a single amino acid change, converting S5 to the non-phosphorylatable alanine. Mice homozygous for the S5A allele are viable and develop normally. In contrast to many prior reports, we found no defects in T or B cell motility or activation, nor in alveolar macrophage production.

Instead, we identified a novel, specific defect in the ability to clear pneumococcal bacteremia. Defective clearance was associated with reduced numbers of splenic MZM and with impaired macrophage- and neutrophil-mediated phagocytosis of pneumococci. Importantly, $LPL^{-/-}$ mice showed no defects in pneumococcal bloodstream clearance, numbers of splenic MZM, or phagocytosis. Our studies thus reveal a physiological requirement for S5 phosphorylation of LPL in the context of host-pathogen interaction, and highlight the essential role of splenic MZM in effective pneumococcal clearance from the blood. Our findings further predict that unexpected, rare and severe immunodeficiencies may arise from single point mutations in actin-binding proteins.

Materials and Methods

Mice

S5A mice were generated with use of a designed sgRNA targeting the change, using the CRISPR/Cas9 system provided by Genome Engineering & iPSC Center (GEIC) at Washington University in St. Louis School of Medicine. The constructs were injected into C57BL/6 embryonic stem cells to minimize the need for further back-crossing. Offspring expressing the S5A mutation were selected by deep sequencing and further back-crossed to wild-type (WT) C57Bl/6 (B6) mice for three generations to eliminate possible CRISPR off-target effects (19) Primers were designed as follows: FW 5’-ctg tca cct aaa gca gtg aaa atg gc- 3’ and Rev 5’ -ctc tga gct cca tca ttt ctt cgt - 3’ for use of deep sequencing to verify inserts. After establishment of the S5A line, subsequent genotyping was performed using allelic discrimination RT-PCR. SNP-PCR probes included Reporter 1 Dye VIC 5’ -c aga gga TCC gtg tct- 3’ as WT Ser5 and Reporter 2 Dye Fam 5’-c aga ggg GCC gtg t- 3’ at Ala5. Quantitative qPCR was carried out using a thermal cycler Applied Biosystems 7500 Fast Real-Time PCR System (Thermo Fisher Scientific) in a Micro Amp Fast Optical 96-Well Reaction Plate, 0.1 mL PCR plate (cat# 4346907; Life Technologies). Amplification for each sample had an identifier to each mouse, and included an empty well as a negative control, in a total volume of 15 μL containing: TaqPath ProAmp Master Mix (cat# A30865; Life Technologies), Custom TaqMan SNP Genotyping Assay Assay Id AHQJU3Q (40X; Fwd & Rev at 36uM; Reporters 8 uM; Thermo Fisher Scientific), 2 μL target DNA at final concentration 5ng/uL. Conditions were carried out as follows: hot start 95 °C for 15 min, then 95 °C for 10 s, 60 °C for 30 s FAM, VIC, ROX (Reference Dye) for 40 cycles.

$LPL^{-/-}$ mice fully back-crossed to the C57Bl/6 background have been described (7, 8). WT and $LPL^{-/-}$ mice were bred and co-housed in the same specific pathogen-free barrier animal facility. Mice matched for sex and age were used in all experiments which were conducted

in accordance with a protocol approved by the WUSM Institutional Animal Care and Use Committee.

While both S5A and LPL$^{-/-}$ mice have been back-crossed to the C57Bl/6 strain, they have been maintained separately and the S5A mice are compared to WT mice generated from the same CRISPR line breeding scheme described above. The WT mice used as controls for the S5A mice are therefore from a genetic lineage different from the C57Bl/6 mice continually co-housed with and bred as WT mice matched to the LPL$^{-/-}$ mice. As such, we have notated control mice for LPL$^{-/-}$ mice as "B6" to distinguish them from the CRISPR-generated "WT" used as matched controls for S5A mice. We grant that theoretically all should be genetically C57Bl/6; in practice, we maintain each CRISPR line with its own littermate matched controls to account for any potential co-housing or breeding variations.

Cell isolation and media

Bronchoalveolar lavage (BAL) was performed as described (7) and cells quantified by flow cytometry (8). Lungs were homogenized using 2.5 mg/ml Collagenase D in Hanks' balanced salt solution (HBSS) + 3% fetal calf serum (FCS) (8).

Immunoblots

Immunoblots were performed as described (6). Membranes were probed with the indicated primary antibodies, anti-LPL and anti-phosphoLPL (provided by Eric J. Brown, Genentech) (20, 21), and actin (D6A8) as loading control (Cell Signaling, Danvers, MA). Goat anti-rabbit-AlexaFluor680 (Invitrogen) and goat anti-mouse-IRDye800 (Rockland Immunochemicals, Gilbertsville, PA) antibodies were used to detect membrane-bound antibodies. Signal was visualized using LiCOR Odyssey imaging system and software (LiCOR, Lincoln, NE).

Confocal microscopy

Tissue-resident intraperitoneal macrophages were harvested as before (22). After 30 m serum starvation, macrophages were stimulated with media containing 10% serum, then fixed in 4% PFA. Following permeabilization with 0.2% Triton X-100, cells were blocked with 5% normal goat serum in PBS, then stained for the indicated markers. Primary antibodies were anti-CD163 (1:100), anti-CD169 (1:100), and CD209b (1:25), and anti-Talin 1 (1:100); secondary antibodies were Alexa Fluor 594 and Alexa Fluor 647 (1:100). F-actin was illuminated with phalloidin-Alexa Fluor 488 (1:500) and the nucleus with DAPI (1:1000). Images were acquired using Zeiss LSM 880 Airyscan Two-Photon Confocal Microscope.

Generation of bone marrow-derived macrophages (BMDMs) and ex vivo intracellular pneumococcal killing assay

Bone marrow was harvested from matched (sex and age) WT and S5A littermate mice and cultured in R10 plus 10% supernatant from L929 cells (R10: RPMI supplemented with 10% FBS, 1 mM Hepes, 1x Glutamax (Life Technologies), 1x Pen/Strep (Life Technologies)) for 7–8 days. Media was refreshed on the third or fourth day of culture. Immediately prior to the *ex vivo* intracellular killing assay, BMDMs are removed from the culture dish with non-

enzymatic CellStripper Dissociation Reagent (Fisher Scientific), washed in PBS and resuspended in fresh media (1×10^5 cells per well).

Pneumococci were prepared for the *ex vivo* intracellular killing assay by serum opsonization (23). Pneumococci (D39) were cultured in Todd Hewitt Broth supplemented with 0.2% yeast extract for four hours, then incubated in R10 with opsonizing serum (1:1) for 10 m. Serum-opsonized D39 were co-incubated with BMDMs at 10–100:1 ratio. After 1 h, supernatant on experimental samples was replaced with R10 plus Pen/Strep and Gentamycin (300 μg/ml) to kill extracellular bacteria. An additional 1 h of incubation with antibiotic-containing media, cells were washed, then lysed (1% saponin x 15 s); for extracellular control samples the final wash was plated for antibiotic efficiency. Lysates were assayed for viable bacteria by serial plate dilution. The ratio between viable bacteria recovered at 1 h (intracellular and externally adhered bacteria) and 2 h (intracellular only) represents effective intracellular killing, and controls for potential differences in phagocytic uptake.

Flow cytometry

Commercial antibodies (clones, fluorophores and sources) are as follows: CD3-FITC (145–2C11), CD62L-PE (Mel-14), CD4-PerCP/Cy5.5 (RM4–5), CD8-PerCP/Cy5.5 (53–6.7), CD8-APC (53–6.7), CD209b-APC (22D1), IgM-FITC (II/41), CD4-PE (GK1.5), CD25-AF488 (PC61.5), Streptavidin-PE, CD169-PE/Cy7 (3D6.112) (eBioscience, San Diego, CA); CD11b-FITC (M1/70), CD49d-FITC (R1–2), TCRβ-FITC (GL3), CD21/35-PE (7E9), CD23-APC (B3B4), Ly6G-PE (RB6–8C5), Ly6C-PerCP/Cy5.5 (HK1.4), CD11c-PE/Cy7 (N418), B220-PerCP/Cy5.5 (RA3–6B2), B220-APC (RA3–6B2), B220-APC/Cy7 (RA3–6B2), CD69-BV421 (H1.2F3),CD23-Biotin (B3B4), F4/80-APC (BM8), Ly6G-BV421 (1A8), CD45-Pacific Blue (30-F11), CD45-BV510 (30-F11), CD43-PE (1B11), CD24-PE/Cy7 (M1/69), IgD-Pacific Blue (11–26c.2a), CD69-PE/Cy7 (H1.2F3), IgD-PerCP/Cy5.5 (11–26c.2a), Ly51-AF647 (6C3), CD3-Pacific Blue (17A2), CD3-PE (17A2), TCRγ/δ-biotin (GL3), Streptavidin-PE/Cy7 (Biolegend, San Diego, CA); Siglec-F-PE (E50–2440) (BD Biosciences, San Jose, CA). Samples were preincubated with 1 μg Fc-block (2.4G2 hybridoma; ATCC).

Cells were acquired either on the BD Biosciences LSR Fortessa or with a BD FACScan flow cytometer with DxP multi-color upgrades by Cytek Development Inc. (Woodland Park, NJ) and analyzed using FlowJo software (FlowJo LLC, Ashland, OR).

Transwell Migration Assays

Transwell inserts (3 or 5 μM; Corning Costar, Lowell, MA) were incubated overnight at 4°C with recombinant murine VCAM-1-Fc chimera (R&D Systems, Minneapolis, MN) and washed with sterile PBS. Transmigration assays were performed as described (6) with CXCL12 (R&D Systems). Whole (unseparated) single cell splenocyte suspensions were used. After incubation for 3–4 h at 37°C, cells were recovered from the lower chamber and counted using a hemocytometer with subpopulations determined by flow cytometry. Percentage of migrated cells was determined by dividing the number of migrated cells, gated as indicated, by the total number of equivalently gated input cells.

Upregulation of activation markers and proliferation

$CD3^+$ (T cells) or $B220^+$ (B cells) cells isolated (Miltenyi Biotec, Inc, per manufacturers' directions) from WT or S5A splenocytes were incubated overnight with anti-CD3 (1 μg/ml; 145–2C11, eBioscience)/anti-CD28 (1 μg/ml; 37.51, eBioscience) (T cells) or plate-bound anti-IgM 10 μg/ml; F(ab')2 fragment of goat anti-mouse IgM, Jackson ImmunoResearch, West Grove, PA) (B cells). Upregulation of CD69 and CD86 was assessed by flow cytometry (6, 24).

For proliferation assays, $CD3^+$ (T cells) or $B220^+$ cells (B cells) isolated from WT or S5A splenocytes using negative selection (Miltenyi Biotec Inc.) and were labeled with CTV (Invitrogen). Cells were incubated for 72 h in the absence or presence of anti-CD3/anti-CD28 (T cells) or of soluble anti-IgM stimulation (10 μg/ml; F(ab')2 fragment of goat anti-mouse IgM, Jackson ImmunoResearch, West Grove, PA), and rIL-4 (10 ng/ml, R&D Systems) (B cells). Cells were analyzed for CTV dilution by flow cytometry.

Infections

Streptococcus pneumoniae (ATCC 6303; serotype 3; 5×10^4 cfu/animal in 20 μl DPBS) was instilled into mice via i.t. injection as before (7, 8) for lung challenge. Bloodstream infection, *Streptococcus pneumoniae* (ATCC 6303; serotype 3; 1×10^5–10^6 cfu/animal in 100 μl DPBS) was injected i.v. Bacteria was grown overnight and resuspended the following day in DPBS for injection. For determining bloodstream infection, S.P.6303 CFU diluted blood was plated on Trypticase™ Soy Agar with 5% Sheep Blood (TSA II; Fisher Scientific) and counted.

Blood was obtained 24 h after challenge for quantitative culture. Mice were monitored at least twice daily with clinical condition scored using a "humane endpoints" scoring system that included daily weight and temperature monitoring and observation of animals grooming, activity, behavior and respirations. Animals that lost > 20% of starting weight or that scored ≥ 5 on the clinical observation score were euthanized.

Tissues were harvested for either flow cytometry or for histology. Histological specimens were preserved in formalin (10%) for 24hr, transferred to 70% Ethanol, then embedded in paraffin. Sections were prepared and stained by hematoxylin and eosin by the Division of Comparative Medicine core facility at WUSM. Pathological reports were reported in a blinded fashion by Dr. Suellen C. Greco, DVM, DACLAM.

Immunofluorescence

To image bacterial capture in the spleen, GFP-labeled pneumococci (D39-GFP; 5×10^6 cfu in 100μl DPBS) was injected *i.v.* into each experimental mouse (age matched 10–12 wk), and the spleen was harvested 60 minutes after injection. The tissues were used for either flow cytometry of splenic macrophages or immunofluorescence of splenic tissue cryosection. *S. pneumoniae* D39 was graciously provided by J. Rosch (25), then transformed to express GFP with hlpA-GFP-cat and alpa-mKate-cat constructs graciously provided by J.W. Veening (26). *S. pneumoniae* 6303 could not be used in these experiments because the capsule of 6303 prevents effective transfection and thus GFP expression.

Confocal imaging of splenic tissue was performed using the same procedure as for primary cells. Spleens were frozen into OTC block immediately after harvesting and cryosections generated. The tissue sections were fixed in 4% PFA, permeabilized with 0.2% Triton X-100 in PBS, and blocked with 5% normal goat serum in PBS. Primary antibodies were anti-CD163 (1:100), anti-CD169 (1:100), and anti-CD209b (1:25); secondary antibodies were Alexa Fluor 594 and Alexa Fluor 647 (1:100); and nucleus counter-staining was DAPI (1:1000). Stained tissues were immediately mounted with DAPI-free fluoromount and coverslip. Images were acquired using a NiKon AIRSi confocal Microscope and processed with NIS-Elements Viewer software.

The area of the splenic sections staining positive for the indicated markers in Fig. 4 was quantified using Fiji Software (27). Background was first reduced by applying the “Smooth” and “Despeckle” processes equivalently to all images. The “percent area” function was used to quantify the percent of each image that stained positive, using a set threshold across all images.

Image analysis for co-localization of D39-GFP and splenic resident macrophage lineages was performed using the Colocalization (Colocalization>Coloc 2) tool in Fiji (27) to calculated Pearson’s Coefficient to quantify the degree to which the red (splenic macrophage lineage) and green (pneumococcal) images colocalized in splenic areas with pneumococci. A value of “1” indicates perfect colocalization, while a value of “0” indicates no colocalization. Pearson’s Coefficient is chosen because it is calculated independently of signal intensity.

Statistics

Non-parametric tests were used to compare non-Gaussian data. Comparisons of two groups were made using Mann-Whitney and comparisons of multiple groups used the Kruskal-Wallis test. Box and whisker plots show a median line, with the box representing 25–75% and the whiskers indicating minimum and maximum values. Unless otherwise indicated in the figure legend, scatter plots represent each mouse as a symbol with lines showing median values. A p-value of < 0.05 was considered statistically significant. The number of animals and replicates for each experiment is provided in the figure or figure legend.

Results

L-plastin is a 66 kDa actin-bundling protein containing an N-terminal “regulatory” headpiece and two C-terminal actin-binding domains. Multiple regulatory elements in the N-terminal region have been described, including phosphorylation sites at serine 5 (S5), serine 7 (S7) and threonine 89 (T89), calcium-binding EF-domains, and a calmodulin-binding domain (Fig. 1A). Most prior research has focused on phosphorylation of S5 as the primary regulatory element of actin-binding by LPL. However, data have been largely correlative, and recent reports suggest that phosphorylation only at S5 may be insufficient to alter actin-binding or actin-bundling (17, 18). To define the *in vivo* function of S5 phosphorylation, we used CRISPR technology to generate mice that express endogenous full-length LPL with a single nucleotide change converting S5 to a non-phosphorylatable alanine (S5A; Fig. 1B). Mice homozygous for the S5A LPL variant are referred to hereafter as “S5A” mice. Control

animals are wild-type (WT) mice generated from the same back-crosses of CRISPR animals and B6 mice.

Expression of non-phosphorylated LPL in S5A mice was confirmed by immunoblot of splenocytes from S5A, matched WT, and unrelated $LPL^{-/-}$ mice (Fig. 1C). As expected, cells from WT mice expressed LPL with constitutive S5 phosphorylation, while cells from $LPL^{-/-}$ animals expressed no LPL protein. Cells from S5A mice expressed endogenous LPL protein at levels comparable to WT, but without detectable S5 phosphorylation. Initial analysis of F-actin morphology of residential peritoneal macrophages revealed no dramatic disruptions of morphology or podosome formation (Fig. 1D). Thus, we successfully generated mice expressing endogenous LPL that cannot be S5 phosphorylated.

We have previously shown that $LPL^{-/-}$ mice exhibit impairments in thymocyte egress and in mature T cell activation (20, 21), and others have reported that the S5 phosphorylation site of LPL regulated CD69 export following TCR engagement (12). Impaired motility and synapse formation in $LPL^{-/-}$ mice was associated with functional impairment of the actin cytoskeleton (20, 21). However, we found no alteration in thymocyte populations (Supp. Fig. 1A) or in T cell activation by anti-CD3 and anti-CD28, as assessed by CD69/CD25 upregulation (Supp. Fig 1B) and T cell proliferation (Supp. Fig. 1C). Assays of B cell development (Supp. Fig. 1D, 1E, 1F) and B cell proliferation following BCR+IL-4 *in vitro* stimulation (Supp. Fig. 1G) did not show the defects of MZB cell development and B cell activation seen previously in $LPL^{-/-}$ mice (6). No differences in proportions of leukocytes circulating in peripheral blood were observed (Supp. Fig. 1H). In Transwell assays, migration of T and B cells derived from S5A mice was equivalent to those from WT mice (Supp. Fig. 2), in contrast to the impaired migration of $LPL^{-/-}$ lymphocytes (5, 6, 20). Additionally, normal migration of S5A lymphocytes differs from the prior observation that ablation of LPL S5 phosphorylation reduced migration of non-hematopoietic HEK293T cells, when WT and S5A LPL were compared in an over-expression system (10).

We next assessed AM development and function in S5A mice, because we have shown that LPL is essential to normal AM production and pneumococcal clearance from the lungs (7, 8). Reduced numbers of AMs in $LPL^{-/-}$ mice was associated with impaired migration, an F-actin dependent process (8). Flow cytometric analysis of bronchoalveolar (BAL) fluid (Fig. 2A, B) and whole lung homogenates (Fig. 2B) obtained from WT and S5A mice revealed no difference in AM percentage or numbers. Additionally, no difference in percentage of eosinophils, dendritic cells, T or B cell were noted in whole lung homogenates (Fig. 2B). AM function was tested by challenging WT and S5A mice via intra-tracheal instillation of pneumococcus (7, 8). Pneumococcal burden, as quantified by colony-forming units in lung homogenates 24 h after instillation, was equivalent in WT and S5A mice (Fig. 2C), differentiating S5A mice from $LPL^{-/-}$ mice (7). Intriguingly, we noted a trend towards a greater percentage of bacteremic S5A mice following pulmonary infection (although the difference did not reach statistical significance), despite equivalent lung bacterial burdens (Fig. 2D). *Ex vivo* analysis of bone marrow derived macrophages obtained from WT and S5A mice incubated with pneumococci showed no difference in intracellular bacterial killing (Fig. 2E). Either S5A mice were more likely to become bacteremic after lung challenge, or

bacteremia is common after lung challenge but is cleared more readily in WT mice than in S5A mice, through a mechanism other than a difference in intracellular killing.

To directly test the ability of WT and S5A mice to clear pneumococcal bacteremia, WT, S5A and LPL$^{-/-}$ mice were directly challenged via intravenous (i.v.) injection of pneumococcus. S5A mice harbored significantly higher bacterial burden in blood 24 h after injection (Fig. 3A), compared to both WT and LPL$^{-/-}$ mice. Notably, the clearance defect in S5A mice was not present in LPL$^{-/-}$ mice, indicating that the molecular dysregulation induced by ablation of LPL S5 phosphorylation is distinct from the molecular dysregulation induced by LPL deficiency. The spleen is the major organ responsible for clearing the blood of bacteria, particularly encapsulated organisms such as pneumococci (3). Therefore, we analyzed the splenic histology of WT and S5A mice 72 h after i.v. pneumococcal infection. Histology of S5A spleens revealed massive apoptosis of splenic white pulp (Fig. 3B), suggesting uncontrolled infection. To confirm that the cleared areas were due to apoptosis, we performed flow cytometric analysis of spleens of WT, S5A, and LPL$^{-/-}$ mice 72 h after pneumococcal bacteremia. Analysis revealed significant loss of B cell populations, most notably of MZB cells (Fig. 3C, D), in S5A compared to WT mice. LPL$^{-/-}$ mice lack MZB cells at baseline (Fig. 3C) so a post-infectious response could not be evaluated (6). Additionally, MZB cells in S5A mice exhibited increased surface labeling with Annexin-V, a marker of apoptosis (Fig. 3E).

Because splenic damage in S5A (but not in WT or LPL$^{-/-}$ mice) resulted in loss of control of pneumococcal infection, we next evaluated the populations of splenic immune cells known to respond immediately to bloodstream pneumococcal infection. The three tissue-resident splenic macrophage populations include red pulp macrophages (RPM), marked by CD163 and residing scattered throughout the red pulp; MMM, marked by CD169 and residing in a layer surrounding the follicle; and MZM, marked by CD209b and residing within the splenic marginal zone (Fig. 4A). As deficiencies in either MZM and/or MMM could contribute to defective splenic pneumococcal clearance (28–30), we compared RPM, MZM, and MMM populations in the spleens from WT, S5A and LPL$^{-/-}$ mice. Because LPL$^{-/-}$ mice demonstrated no defect in bacterial bloodstream clearance, we assessed for differences between S5A and WT littermate controls that were not present between LPL$^{-/-}$ and matched B6 controls. Immunofluorescence microscopy of splenic sections from WT, S5A, LPL$^{-/-}$, and the B6 mice suggested reduced MZM in S5A mice compared to littermate WT controls (Fig. 4B). There was no observed reduction in any splenic macrophage lineage in LPL$^{-/-}$ spleens compared to B6 controls.

We quantified the area of each field that stained positive for the indicated markers as an initial surrogate to define potential differences in macrophage lineages (Supp. Fig 3A). However, we found that this measurement varied greatly between randomly selected sections within each spleen. Therefore, we used flow cytometry to definitively quantify the population of each macrophage lineages in whole splenic homogenates to compare populations between WT, S5A, LPL$^{-/-}$ and B6 mice.

Flow cytometric analysis of macrophage lineages (defined as in Supp. Fig 4) after splenic collagenase digestion (Fig. 5A) revealed a significant reduction in the percentage of MZM

cells in spleens from S5A mice compared to WT. The percentages of RPM and MMM were equivalent. There was no reduction in percentages of MZM, RPM, or MMM lineages in LPL $^{-/-}$ mice compared to their matched B6 controls (Fig. 5B).

We also evaluated if a *functional* defect in innate immune cells could contribute to the failure to clear pneumococcal bloodstream infections. Although we previously found no evidence for defective pneumococcal phagocytosis by AMs in LPL$^{-/-}$ mice (7), impaired phagocytosis by expression of S5A LPL could result in failure to control pneumococcal bacteremia, despite effective killing (Fig. 2E). To test for a defect in phagocytosis, we injected GFP-tagged pneumococci strain D39 i.v. into S5A, LPL$^{-/-}$, and respective control mice and reviewed splenic histology (Fig. 6). Splenic macrophage lineages were identified as in Fig. 4B. Co-localization (yellow) of pneumococci (green) with MZM (red) in spleens of S5A mice qualitatively appeared reduced compared to analogous co-localization in WT controls. However, co-localization of RPM and MMM lineages with pneumococci appeared equivalent in S5A and matched controls. Additionally, co-localization of pneumococci with all macrophage lineages in spleens from LPL$^{-/-}$ mice appeared similar to that of matched B6 controls (Fig. 6). We first quantified the degree of colocalization observed in each randomly-selected splenic section using Pearson's Coefficient (Supp. Fig. 3B), but again found a large degree of variability between fields, even within the same splenic section (Supp. Fig. 3B), and definitive quantification was performed using flow cytometry. These observations suggest that beyond a reduced MZM population, S5A mice also exhibit a functional defect in the ability of MZM to capture pneumococci.

To quantify the possible functional defect of MZM from S5A mice suggested by microscopy, we analyzed the percentage of MZM, RPM, MMM, and other innate immune cells that acquired GFP signal (i.e., took up pneumococci) following bloodstream infection with D39-GFP by flow cytometric analysis (Fig. 7). While the absolute uptake of bacteria varied among experiments, the percent of MZM, MMM, neutrophils and monocytes positive for D39-GFP was consistently and significantly reduced in S5A mice compared to WT control mice from each experiment (Fig. 7A). Notably, there was no consistent increase or decrease in the percent of RPM positive for D39-GFP (Fig. 7A), indicating that the impairment in phagocytosis was lineage specific. Furthermore, we again found no evidence for a defect in bacterial uptake in any phagocytic lineage in LPL$^{-/-}$ mice (Fig. 7B), consistent with our prior results (7). Thus, ablation of S5 phosphorylation specifically impaired uptake of bacteria in certain phagocytic lineages, while complete lack LPL did not inhibit phagocytosis.

Discussion

In summary, we have generated a new mouse model to convert serine 5 of LPL to alanine and thereby prevent phosphorylation. We used these mice to test the hypothesis that S5 phosphorylation of LPL was a major regulatory site that governs leukocyte motility and development. We did not find *in vivo* evidence supporting that S5 phosphorylation alone governed T cell motility, development or activation; B cell motility, development, or activation; or AM development (Fig. 1, 2), as suggested either by prior literature or by phenotypes previously observed in LPL$^{-/-}$ mice (5–8, 12, 13, 20, 21, 31). However, we did

identify two highly specific defects in splenic MZM population frequency and in pneumococcal phagocytosis by neutrophils, monocytes and splenic MZM and MMM. Defects in splenic macrophage populations and in phagocytosis distinguish the S5A mouse from $LPL^{-/-}$ mice, as complete loss of LPL does not affect MZM frequency or phagocytosis (Fig. 5, 7). The narrow functional deficiencies in the S5A splenic cells resulted in a specific host immune weakness to pneumococcal bloodstream infection, even while S5A mice clear lung infection normally (Fig. 2, 3). The S5A mouse thus offers a novel model system to further understand how actin-binding proteins play key roles in specific immune functions essential to host defense, and reveal the exquisite sensitivity of specific host-pathogen interactions to subtle genetic changes, in this case a single-residue variant in a leukocyte protein.

The novel S5A mice highlight the key importance of splenic tissue-resident macrophages in anti-pneumococcal host defense. The marginal zone has long been recognized as the critical location for capture of polysaccharide antigens (32, 33). One of the first studies to investigate pneumococcal clearance revealed prompt capture in the marginal zone within 15 min of i.v. injection (34). The only cell lineage reduced in population in S5A mice were the $CD209b^{+}$ MZM (Supp. Fig 1, Fig. 4B). Because of their location along the sinuses, and the relatively slow transit of blood through the MZ, MZM are uniquely positioned to screen the bloodstream for pathogens. Furthermore, MZM specifically express CD209b (also termed SIGNR1), a C-type lectin that binds the polysaccharide capsule of pneumococcus (28). Deletion of SIGN-R1 has been previously shown to severely impair splenic uptake of pneumococcus and increase mortality during pneumococcal bacteremia (32).

A second defect in host defense in S5A mice was apparent in diminished phagocytic capacity of multiple innate cell lineages (Fig. 6, 7). Our initial observation that LPL was dispensable for phagocytosis was somewhat surprising, as the homologous yeast actin-bundling protein Sac6 had been demonstrated to be required for endocytosis (35, 36). Additionally, FcγRII-mediated phagocytosis induced phosphorylation of LPL, suggesting LPL would be involved in the phagocytic process (37). However, our data here clearly support a model in which LPL is dispensable for phagocytosis, but expression of the nonphosphorylatable S5A-LPL inhibits pneumococcal internalization in a lineage-specific manner (Fig. 7). (Of note, the BMDMs from S5A mice appear similar to splenic RPMs, in that phagocytosis of pneumococci is equivalent to WT (Fig. 2E).) The most parsimonious explanation is that S5A-LPL acts in a dominant negative manner, while complete loss of LPL can be compensated by other actin-bundling proteins. Continued investigation in the S5A mouse will facilitate elucidation of the exact mechanism.

The S5 phosphorylation site distinguishes LPL from the other two mammalian plastin isoforms. LPL is thought to be the sole plastin expressed in leukocytes, while I-plastin is expressed in kidney and intestinal epithelia and T-plastin is expressed broadly in all nucleated cells outside of the hematopoietic system (31, 38). All three plastins are comprised of an N-terminal “headpiece” regulatory domain followed by two C-terminal actin-binding domains (ABD1 and ABD2). Common to all three plastins are shared regulatory elements in the N-terminal domain, as all have a conserved putative threonine phosphorylation site at residue 89 (39), as well as calcium-binding domains (18, 40). While only LPL contains the

S5 (and neighboring S7 site), functional studies have yet to clearly define the regulatory role for this phosphorylation event. While an earlier paper creating a phosphomimetic S5E-LPL argued that S5 phosphorylation increased LPL actin-binding when overexpressed in Vero or HEK293T cells (10), more recent, extensive *in vitro* analysis using an S5D-LPL phosphomimetic failed to find evidence to support regulation of actin-binding or actin-bundling by S5 phosphorylation (18). The recent work parallels the earliest analysis of LPL phosphorylation in neutrophils, in which S5 phosphorylation correlated with FcγRII phagocytosis, but not with localization to detergent-stable, actin-rich podosomes (37). The data from neutrophils suggested that calcium binding regulates association of LPL with actin-rich sites, consistent with the *in vitro* data showing that calcium binding regulates LPL actin-binding and actin-bundling activities. Data from both Schwebach *et al.* and from Jones and Brown suggest that S5 phosphorylation of LPL regulates a function distinct from pure actin-binding, and in fact may require additional (as yet unidentified) binding partners.

Many publications have observed S5 phosphorylation of LPL in response to multiple cell stimuli, and thereby linked LPL S5 phosphorylation with increased motility or cell activation. However, these studies are either correlative, or performed *in vitro*, or with mutant forms of LPL overexpressed in cell lines (5, 10, 12–14, 16, 41, 42). Our S5A mouse is distinguished from these prior systems in that LPL is expressed at endogenous levels in naive cells under normal physiological conditions. Phosphorylation at S5 was dispensable for many phenotypes that we predicted would be affected based on prior reports, including T and B cell motility, T and B cell activation, and AM development (5–8, 12, 13, 20, 21, 31). Notably, all of these leukocyte functions have been previously linked to effective regulation of F-actin. Unimpaired motility and activation strongly suggests largely unimpaired F-actin cytoskeletal disruption in examined lineages in S5A mice. It is likely that because S5 phosphorylation is, in fact, dispensable for actin-binding and actin-bundling, it is dispensable for these previously correlated phenotypes. Alternatively, in other reports, phosphorylation of the nearby S7 partially compensates for S5 phosphorylation, and ablation of both S5 and S7 was needed to alter LPL function (17). Future work will assess whether S7 phosphorylation is enhanced in cells derived from S5A mice, and if dual phosphorylation at S5 and S7 alters or enhances LPL activity compared to single phosphorylation at either site.

LPL is a critical component of the macrophage podosome (22)). Podosomes are integrin-anchored, actin-based multimolecular complexes containing up to 200 proteins. Podosomes are signaling organelles supporting monocyte and macrophage motility and adhesion (43, 44). Ultrastructurally, integrins, integrin-associated adaptors such as talin, and signaling molecules including tyrosine kinases (*e.g.* Src-family, Pyk2) form an adhesive “ring” surrounding a “core” of bundled F-actin (45). F-actin cross-linked by myosin links the ring and core components. While LPL is essential for podosome stability (8, 22, 44), the precise role of LPL in podosome fomration has yet to be clearly defined. LPL may bundle the actin filaments of the podosome core (46), or may serve a role in integrin-based signaling (47). While we have not yet uncovered podosome formation defects in macrophages from S5A mice, the specific impairments of MZM population frequency and phagocytic defects in select myeloid lineages suggest that S5A may disrupt integrin-signaling or adhesion. The

S5A mice thus provide a model system in which to further explore in detail the molecular mechanism(s) supported by LPL in podosome stability and function.

In summary, generation of the novel S5A LPL mouse contributes to our understanding in three ways. First, we have established that phosphorylation of LPL at S5 is not required for many of the phenotypes which have been previously correlated with LPL phosphorylation, demonstrating the necessity of testing causality in physiological systems with proteins expressed at endogenous levels. Second, we have identified novel and unexpected phenotypes previously unknown to be LPL-dependent: first, the population of MZM is uniquely dependent on LPL phosphorylation (but neighboring MZB and other splenic tissue-resident macrophages are not), and phagocytosis is inhibited by the expression of non-phosphorylatable LPL. Future work detailing the mechanisms underpinning these phenotypes will illuminate these critical immune processes. Third, these mice will enable the further delineation of how components, such as calcium-binding (18) and T89 phosphorylation (39), of LPL regulation are coordinated, and will support the identification of intracellular binding partners that facilitate the specific roles of LPL within each hematopoietic cell type. Most importantly, the singular impairment of S5A mice in clearing pneumococcal bacteremia, but not pneumococcal lung infection, reveals how a severe and specific immunodeficiency might result from a non-obvious point mutation.

Supplementary Material

Refer to Web version on PubMed Central for supplementary material.

Acknowledgements

The authors thank P.J. Stewart-Hutchinson and Darren Kreamalmeyer for technical assistance with generation of the S5A mice and support of the mouse colony. We thank David A. Hunstad for critical review of the manuscript.

S.C.M. was supported by the National Institutes of Health (R01-AI104732; R56 AI104732). This work was supported by the Hope Center Transgenic Vectors Core at Washington University School of Medicine. Experimental support was also provided by the Speed Congenics Facility of the Rheumatic Diseases Core Center. Research reported in this publication was supported by the National Institute of Arthritis and Musculoskeletal and Skin Diseases, part of the National Institutes of Health, under Award Number P30-AR048335.

2Abbreviations:

LPL	L-plastin
WT	wild-type
BAL	bronchoalveolar lavage
S5	serine 5
S5A	serine 5 to alanine
MZ	marginal zone
MZB	marginal zone B cells
MZM	marginal zone macrophages

MMM	metallophilic macrophages
RPM	red pulp macrophages
AM	alveolar macrophages
B6	C57Bl/6 mouse line
PMNs	polymorphonuclear cells

References

1. O'Brien KL, Wolfson LJ, Watt JP, Henkle E, Deloria-Knoll M, McCall N, Lee E, Mulholland K, Levine OS, and Cherian T. 2009. Burden of disease caused by Streptococcus pneumoniae in children younger than 5 years: global estimates. Lancet 374: 893–902. [PubMed: 19748398]
2. Chiou CC, and Yu VL. 2006. Severe pneumococcal pneumonia: new strategies for management. Curr. Opin. Crit. Care 12: 470–476. [PubMed: 16943728]
3. Lammers AJ, de Porto AP, Florquin S, de Boer OJ, Bootsma HJ, Hermans PW, and van der Poll T. 2011. Enhanced vulnerability for Streptococcus pneumoniae sepsis during asplenia is determined by the bacterial capsule. Immunobiology 216: 863–870. [PubMed: 21397979]
4. Mebius RE, and Kraal G. 2005. Structure and function of the spleen. Nat. Rev. Immunol 5: 606–616. [PubMed: 16056254]
5. Freeley M, O'Dowd F, Paul T, Kashanin D, Davies A, Kelleher D, and Long A. 2012. L-Plastin Regulates Polarization and Migration in Chemokine-Stimulated Human T Lymphocytes. J. Immunol 188: 6357–6370. [PubMed: 22581862]
6. Todd EM, Deady LE, and Morley SC. 2011. The actin-bundling protein L-plastin is essential for marginal zone B cell development. J. Immunol 187: 3015–3025. [PubMed: 21832165]
7. Deady LE, Todd EM, Davis CG, Zhou JY, Topcagic N, Edelson BT, Ferkol TW, Cooper MA, Muenzer JT, and Morley SC. 2014. L-plastin is essential for alveolar macrophage production and control of pulmonary pneumococcal infection. Infect. Immun 82: 1982–1993. [PubMed: 24595139]
8. Todd EM, Zhou JY, Szasz TP, Deady LE, D'Angelo JA, Cheung MD, Kim AH, and Morley SC. 2016. Alveolar macrophage development in mice requires L-plastin for cellular localization in alveoli. Blood 128: 2785–2796. [PubMed: 27758872]
9. Todd EM, Ramani R, Szasz TP, and Morley SC. 2019. Inhaled GM-CSF in neonatal mice provides durable protection against bacterial pneumonia. Sci Adv 5: eaax3387. [PubMed: 31453341]
10. Janji B, Giganti A, De Corte V, Catillon M, Bruyneel E, Lentz D, Plastino J, Gettemans J, and Friederich E. 2006. Phosphorylation on Ser5 increases the F-actin-binding activity of L-plastin and promotes its targeting to sites of actin assembly in cells. J. Cell Sci 119: 1947–1960. [PubMed: 16636079]
11. Ishida H, Jensen KV, Woodman AG, Hyndman ME, and Vogel HJ. 2017. The Calcium-Dependent Switch Helix of L-Plastin Regulates Actin Bundling. Sci. Rep 7: 40662. [PubMed: 28145401]
12. Wabnitz GH, Kocher T, Lohneis P, Stober C, Konstandin MH, Funk B, Sester U, Wilm M, Klemke M, and Samstag Y. 2007. Costimulation induced phosphorylation of L-plastin facilitates surface transport of the T cell activation molecules CD69 and CD25. Eur. J. Immunol 37: 649–662. [PubMed: 17294403]
13. Wabnitz GH, Michalke F, Stober C, Kirchgessner H, Jahraus B, van den Boomen DJ, and Samstag Y. 2011. L-plastin phosphorylation: a novel target for the immunosuppressive drug dexamethasone in primary human T cells. Eur. J. Immunol 41: 3157–3169. [PubMed: 21805466]
14. Dubovsky JA, Chappell DL, Harrington BK, Agrawal K, Andritsos LA, Flynn JM, Jones JA, Paulaitis ME, Bolon B, Johnson AJ, Byrd JC, and Muthusamy N. 2013. Lymphocyte cytosolic protein 1 is a chronic lymphocytic leukemia membrane-associated antigen critical to niche homing. Blood 122: 3308–3316. [PubMed: 24009233]
15. De Clercq S, Zwaenepoel O, Martens E, Vandekerckhove J, Guillabert A, and Gettemans J. 2013. Nanobody-induced perturbation of LFA-1/L-plastin phosphorylation impairs MTOC docking,

immune synapse formation and T cell activation. Cell. Mol. Life Sci. : CMLS 70: 909–922. [PubMed: 23001012]

16. Lommel MJ, Trairatphisan P, Gabler K, Laurini C, Muller A, Kaoma T, Vallar L, Sauter T, and Schaffner-Reckinger E. 2016. L-plastin Ser5 phosphorylation in breast cancer cells and in vitro is mediated by RSK downstream of the ERK/MAPK pathway. FASEB J. 30: 1218–1233. [PubMed: 26631483]
17. Chellaiah MA, Majumdar S, and Aljohani H. 2018. Peptidomimetic inhibitors of L-plastin reduce the resorptive activity of osteoclast but not the bone forming activity of osteoblasts in vitro. PLoS One 13: e0204209. [PubMed: 30248139]
18. Schwebach CL, Agrawal R, Lindert S, Kudryashova E, and Kudryashov DS. 2017. The Roles of Actin-Binding Domains 1 and 2 in the Calcium-Dependent Regulation of Actin Filament Bundling by Human Plastins. J. Mol. Biol 429: 2490–2508. [PubMed: 28694070]
19. Parikh BA, Beckman DL, Patel SJ, White JM, and Yokoyama WM. 2015. Detailed phenotypic and molecular analyses of genetically modified mice generated by CRISPR-Cas9-mediated editing. PLoS One 10: e0116484. [PubMed: 25587897]
20. Morley SC, Wang C, Lo WL, Lio CW, Zinselmeyer BH, Miller MJ, Brown EJ, and Allen PM. 2010. The actin-bundling protein L-plastin dissociates CCR7 proximal signaling from CCR7-induced motility. J. Immunol 184: 3628–3638. [PubMed: 20194718]
21. Wang C, Morley SC, Donermeyer D, Peng I, Lee WP, Devoss J, Danilenko DM, Lin Z, Zhang J, Zhou J, Allen PM, and Brown EJ. 2010. Actin-bundling protein L-plastin regulates T cell activation. J. Immunol 185: 7487–7497. [PubMed: 21076065]
22. Zhou JY, Szasz TP, Stewart-Hutchinson PJ, Sivapalan J, Todd EM, Deady LE, Cooper JA, Onken MD, and Morley SC. 2016. L-Plastin promotes podosome longevity and supports macrophage motility. Mol. Immunol 78: 79–88. [PubMed: 27614263]
23. Lachmann PJ 2010. Preparing serum for functional complement assays. J. Immunol. Methods 352: 195–197. [PubMed: 19909755]
24. Morley SC, Weber KS, Kao H, and Allen PM. 2008. Protein kinase C-theta is required for efficient positive selection. J. Immunol 181: 4696–4708. [PubMed: 18802072]
25. Rowe HM, Karlsson E, Echlin H, Chang TC, Wang L, van Opijnen T, Pounds SB, Schultz-Cherry S, and Rosch JW. 2019. Bacterial Factors Required for Transmission of Streptococcus pneumoniae in Mammalian Hosts. Cell Host Microbe 25: 884–891 e886. [PubMed: 31126758]
26. Kjos M, Aprianto R, Fernandes VE, Andrew PW, van Strijp JA, Nijland R, and Veening JW. 2015. Bright fluorescent Streptococcus pneumoniae for live-cell imaging of host-pathogen interactions. J. Bacteriol 197: 807–818. [PubMed: 25512311]
27. Schindelin J, Arganda-Carreras I, Frise E, Kaynig V, Longair M, Pietzsch T, Preibisch S, Rueden C, Saalfeld S, Schmid B, Tinevez JY, White DJ, Hartenstein V, Eliceiri K, Tomancak P, and Cardona A. 2012. Fiji: an open-source platform for biological-image analysis. Nat. Methods 9: 676–682. [PubMed: 22743772]
28. Kang YS, Kim JY, Bruening SA, Pack M, Charalambous A, Pritsker A, Moran TM, Loeffler JM, Steinman RM, and Park CG. 2004. The C-type lectin SIGN-R1 mediates uptake of the capsular polysaccharide of Streptococcus pneumoniae in the marginal zone of mouse spleen. Proc. Natl. Acad. Sci. U. S. A 101: 215–220. [PubMed: 14694198]
29. Perez OA, Yeung ST, Vera-Licona P, Romagnoli PA, Samji T, Ural BB, Maher L, Tanaka M, and Khanna KM. 2017. CD169(+) macrophages orchestrate innate immune responses by regulating bacterial localization in the spleen. Sci Immunol 2.
30. Ercoli G, Fernandes VE, Chung WY, Wanford JJ, Thomson S, Bayliss CD, Straatman K, Crocker PR, Dennison A, Martinez-Pomares L, Andrew PW, Moxon ER, and Oggioni MR. 2018. Intracellular replication of Streptococcus pneumoniae inside splenic macrophages serves as a reservoir for septicaemia. Nat. Microbiol 3: 600–610. [PubMed: 29662129]
31. Morley SC 2013. The actin-bundling protein L-plastin supports T-cell motility and activation. Immunol. Rev 256: 48–62. [PubMed: 24117812]
32. Lanoue A, Clatworthy MR, Smith P, Green S, Townsend MJ, Jolin HE, Smith KG, Fallon PG, and McKenzie AN. 2004. SIGN-R1 contributes to protection against lethal pneumococcal infection in mice. J. Exp. Med 200: 1383–1393. [PubMed: 15583012]

33. Borges da Silva H, Fonseca R, Pereira RM, Cassado Ados A, Alvarez JM, and D'Imperio Lima MR. 2015. Splenic Macrophage Subsets and Their Function during Blood-Borne Infections. Front. Immunol 6: 480. [PubMed: 26441984]
34. Harms G, Hardonk MJ, and Timens W. 1996. In vitro complement-dependent binding and in vivo kinetics of pneumococcal polysaccharide TI-2 antigens in the rat spleen marginal zone and follicle. Infect. Immun 64: 4220–4225. [PubMed: 8926091]
35. Adams AE, Shen W, Lin CS, Leavitt J, and Matsudaira P. 1995. Isoform-specific complementation of the yeast sac6 null mutation by human fimbrin. Mol. Cell. Biol 15: 69–75. [PubMed: 7799970]
36. Gheorghe DM, Aghamohammadzadeh S, Smaczynska-de R II, Allwood EG, Winder SJ, and Ayscough KR. 2008. Interactions between the yeast SM22 homologue Scp1 and actin demonstrate the importance of actin bundling in endocytosis. J. Biol. Chem 283: 15037–15046. [PubMed: 18400761]
37. Jones SL, and Brown EJ. 1996. FcgammaRII-mediated adhesion and phagocytosis induce L-plastin phosphorylation in human neutrophils. J. Biol. Chem 271: 14623–14630. [PubMed: 8663066]
38. Delanote V, Vandekerckhove J, and Gettemans J. 2005. Plastins: versatile modulators of actin organization in (patho)physiological cellular processes. Acta Pharmacol. Sin 26: 769–779. [PubMed: 15960882]
39. Xu X, Wang X, Todd EM, Jaeger ER, Vella JL, Mooren OL, Feng Y, Hu J, Cooper JA, Morley SC, and Huang YH. 2016. Mst1 Kinase Regulates the Actin-Bundling Protein L-Plastin To Promote T Cell Migration. J. Immunol 197: 1683–1691. [PubMed: 27465533]
40. Namba Y, Ito M, Zu Y, Shigesada K, and Maruyama K. 1992. Human T cell L-plastin bundles actin filaments in a calcium-dependent manner. J. Biochem 112: 503–507. [PubMed: 1491005]
41. Lin CS, Lau A, and Lue TF. 1998. Analysis and mapping of plastin phosphorylation. DNA Cell Biol. 17: 1041–1046. [PubMed: 9881671]
42. Pazdrak K, Young TW, Straub C, Stafford S, and Kurosky A. 2011. Priming of eosinophils by GM-CSF is mediated by protein kinase CbetaII-phosphorylated L-plastin. J. Immunol 186: 6485–6496. [PubMed: 21525390]
43. Messier JM, Shaw LM, Chafel M, Matsudaira P, and Mercurio AM. 1993. Fimbrin localized to an insoluble cytoskeletal fraction is constitutively phosphorylated on its headpiece domain in adherent macrophages. Cell Motil. Cytoskeleton 25: 223–233. [PubMed: 8221900]
44. De Clercq S, Boucherie C, Vandekerckhove J, Gettemans J, and Guillabert A. 2013. L-plastin nanobodies perturb matrix degradation, podosome formation, stability and lifetime in THP-1 macrophages. PLoS One 8: e78108. [PubMed: 24236012]
45. Veillat V, Spuul P, Daubon T, Egana I, Kramer I, and Genot E. 2015. Podosomes: Multipurpose organelles? Int. J. Biochem. Cell Biol 65: 52–60. [PubMed: 26028292]
46. Evans JG, Correia I, Krasavina O, Watson N, and Matsudaira P. 2003. Macrophage podosomes assemble at the leading lamella by growth and fragmentation. J. Cell Biol 161: 697–705. [PubMed: 12756237]
47. Chen H, Mocsai A, Zhang H, Ding RX, Morisaki JH, White M, Rothfork JM, Heiser P, Colucci-Guyon E, Lowell CA, Gresham HD, Allen PM, and Brown EJ. 2003. Role for plastin in host defense distinguishes integrin signaling from cell adhesion and spreading. Immunity 19: 95–104. [PubMed: 12871642]

Key points:

- A new mouse model was made to study the role of Ser-5 phosphorylation of L-plastin
- Ser-5 phosphorylation of L-plastin promoted pneumococcal bloodstream clearance
- Ser-5 phosphorylation of L-plastin was needed for efficient phagocytosis

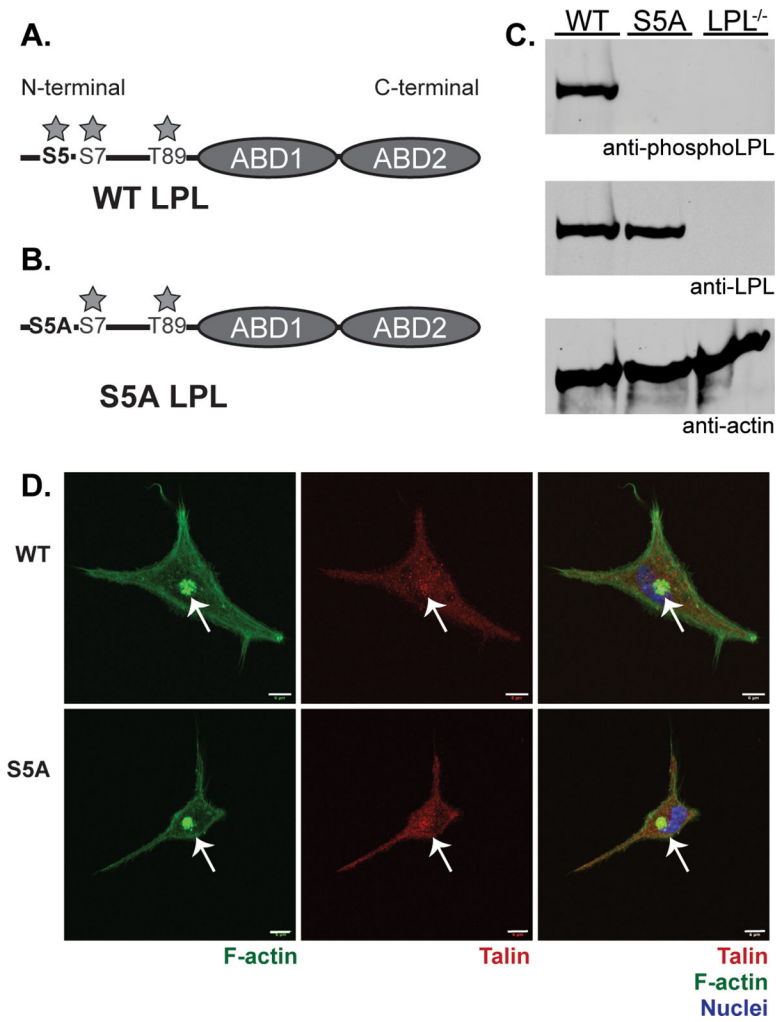

Figure 1. S5A mice express equivalent levels of LPL without evidence of S5 phosphorylation.

A. Schematic of LPL with three identified phosphorylation sites (S5, S7 and T89) in the regulatory N-terminal domain indicated. ABD = actin-binding domain. **B.** Schematic indicating that "S5A" represents endogenous LPL locus in which S5 is converted to non-phosphorylatable alanine residue. **C.** Immunoblot of whole spleen lysates from WT, S5A and $LPL^{-/-}$ mice. Anti-actin immunoblot indicates equivalent protein loading. Anti-LPL immunoblot indicates equivalent expression of endogenous LPL in S5A mice. Specific anti-S5 phosphorylation antibody indicates complete ablation of S5 phosphorylation of native LPL in S5A mice at baseline. **D.** Confocal microscopy of F-actin morphology of residential peritoneal macrophages from WT and S5A mice. F-actin illuminated using phalloidin (green), talin illuminated using anti-talin mAb (red), and nuclei using DAPI (blue). Arrows indicate clusters of podosomes. Scale bar = 6 μm. Images representative of two independent experiments.

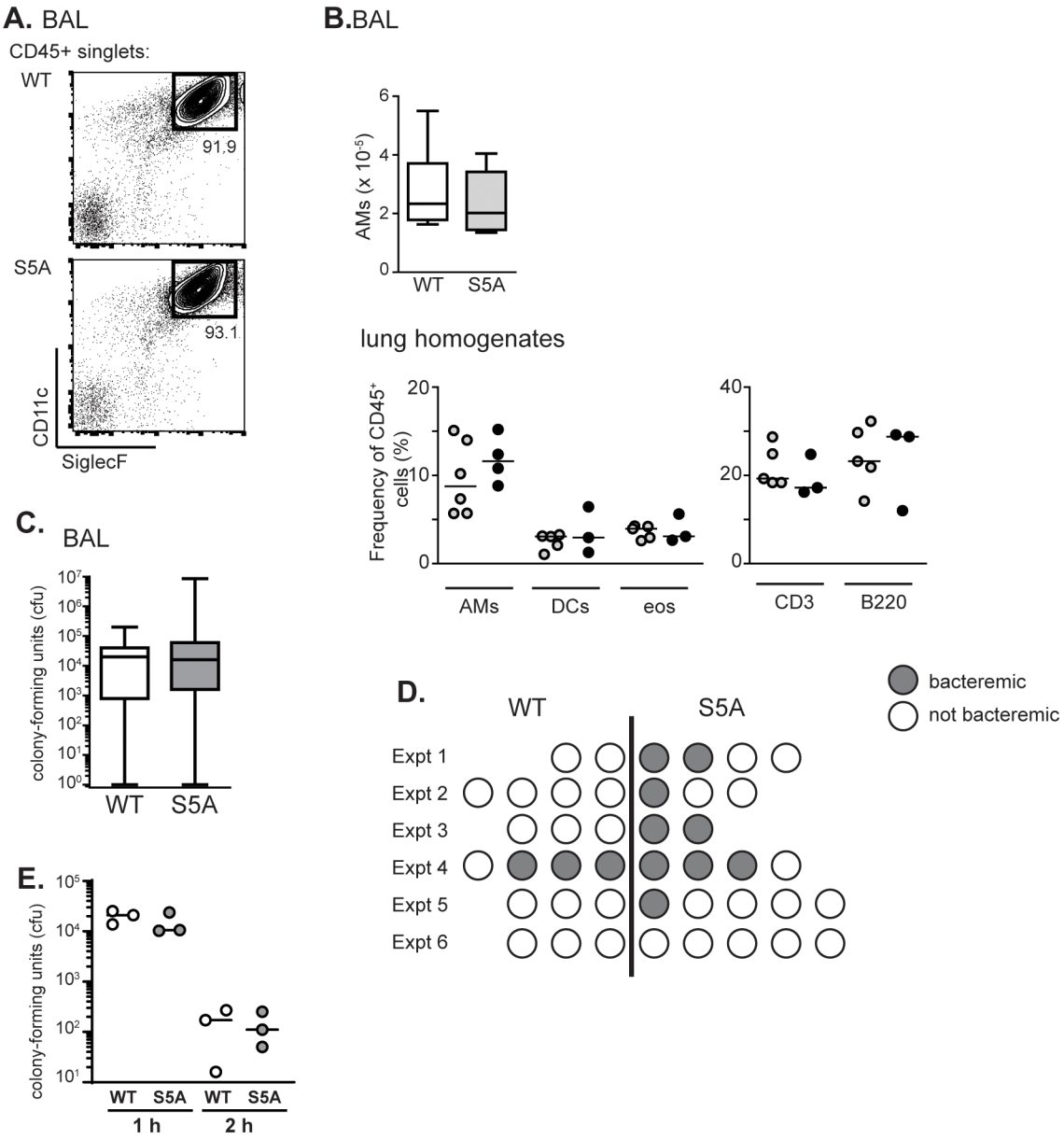

Figure 2. Trend towards increased incidence of pneumococcal bacteremia in S5A mice, despite normal clearance of lung infection.

A. Flow cytometric analysis of bronchoalveolar lavage (BAL) fluid from WT and S5A mice. Gating on $CD11c^{+}/SiglecF^{+}$ cells reveals alveolar macrophages. **B.** Quantification of AMs from BAL fluid from WT (open box, n=6) and S5A (gray box, n=6) mice and frequency of AMs, dendritic cells (DCs), eosinophils (eos), $CD3^{+}$ cells, and $B220^{+}$ cells in whole lung homogenates from WT (open circles) and S5A (gray circles) mice. **C.** Pneumococcal burden (cfu) in BAL fluid from WT (open, n=19) and S5A (gray, n=23) mice 24 h after intra-tracheal instillation. **D.** Incidence of bacteremia in WT and S5A mice 24 h after intra-tracheal instillation in six independent experiments. Each circle represents an individual mouse. Mice in (D) are same as those in (C). **E.** *Ex vivo* pneumococcal killing assay using BMDMs derived from WT (open circles) or S5A (gray circles) mice. Values from triplicates

from representative experiment shown, line at median. Representative of three independent experiments.

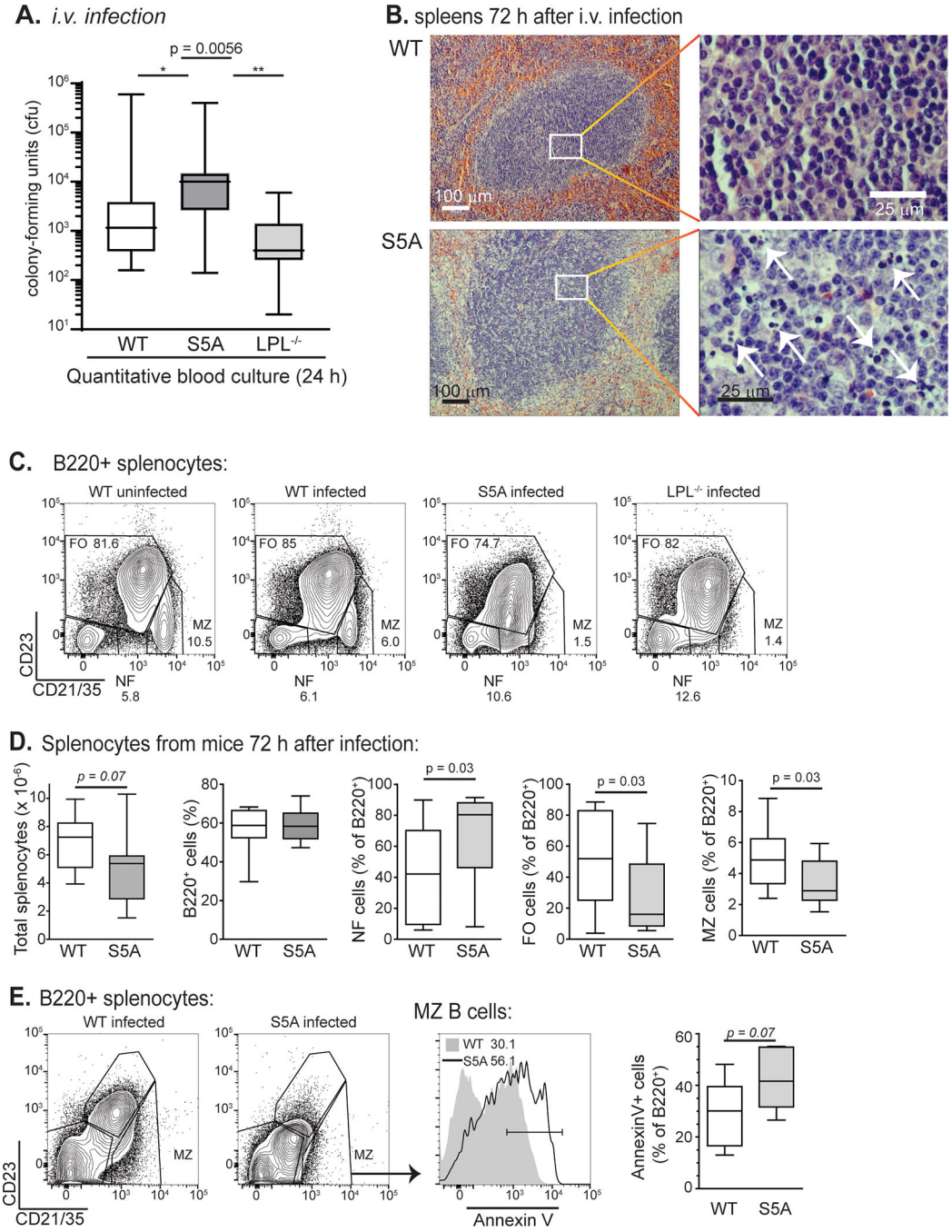

Figure 3. Defective clearance of pneumococcal bacteremia and splenocyte apoptosis in S5A mice.

A. Bacterial burden (cfu) in bloodstream of WT (open, n = 16), S5A (dark gray, n = 17) and LPL$^{-/-}$ (light gray, n = 8) mice 24 h after i.v. challenge with pneumococcus. Kruskal-Wallis ANOVA test, p = 0.0056. Pair-wise comparison of S5A data to WT, $p < 0.05$; S5A to LPL$^{-/-}$, $p < 0.01$ (Dunn's multiple comparison test). B. Spleens from WT and S5A mice isolated 72 h after *i.v.* challenge with pneumococcus revealed increased areas of lymphocyte apoptosis in S5A follicles. C. Flow cytometric analysis of B cell subpopulations from uninfected WT, challenged WT, challenged S5A and challenged LPL$^{-/-}$ mice. MZB cells

are indicated as CD21/35^{high}/CD23^{low}. **D.** Quantification of total splenocytes and B cell subpopulations from WT (open, n = 12) and S5A (gray, n = 12) mice 72 h after pneumococcal *i.v.* challenge. **E.** Flow cytometric analysis and quantification of Annexin-V labeling of MZB cells derived from WT and S5A mice 72 h after challenge with pneumococcus *(i.v.)*.

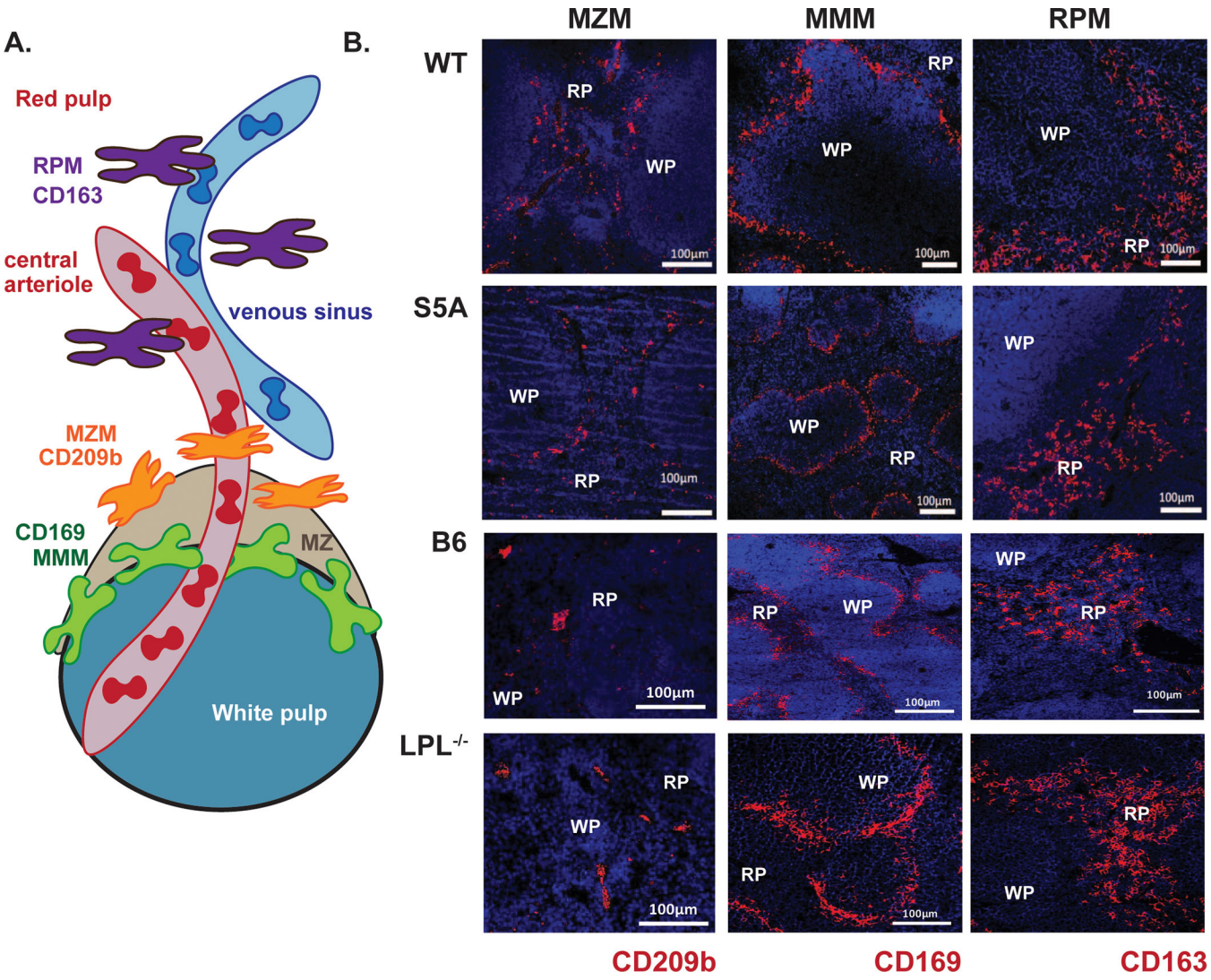

Figure 4. Reduction in MZM splenic population in S5A mice revealed by immunofluorescence.

A. Schematic illustrating three tissue-resident lineages of splenic macrophages. **B.** Immunofluorescence of frozen splenic sections derived from naïve WT, S5A, "B6" and LPL $^{-/-}$ mice. Splenic lineage markers are labeled with anti-CD209b (MZM), anti-CD162 (RPM) and anti-CD169 (MMM; red) and nuclei are counter-stained with DAPI (blue). Scale bars indicate 100 µm. WP = white pulp, RP = red pulp.

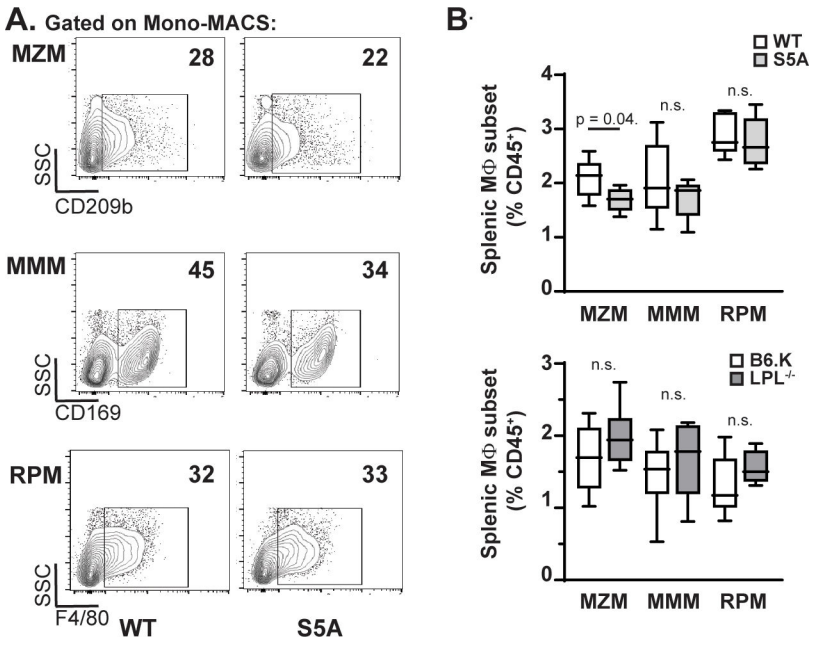

Figure 5. Reduction in MZM splenic population quantified by flow cytometry.

A. Representative flow cytometric analyses of MZM, MMM and RPM populations after gating on all singlet, $CD45^+/CD11b^+$ cells. **B.** Quantification of frequency of MZM, MMM and RPM lineages in S5A mice compared to matched WT controls (upper panel) and in LPL $^{-/-}$ mice compared to matched B6.K controls (lower panel). Frequency of macrophage lineages calculated as percentage of all $CD45^+$ cells.

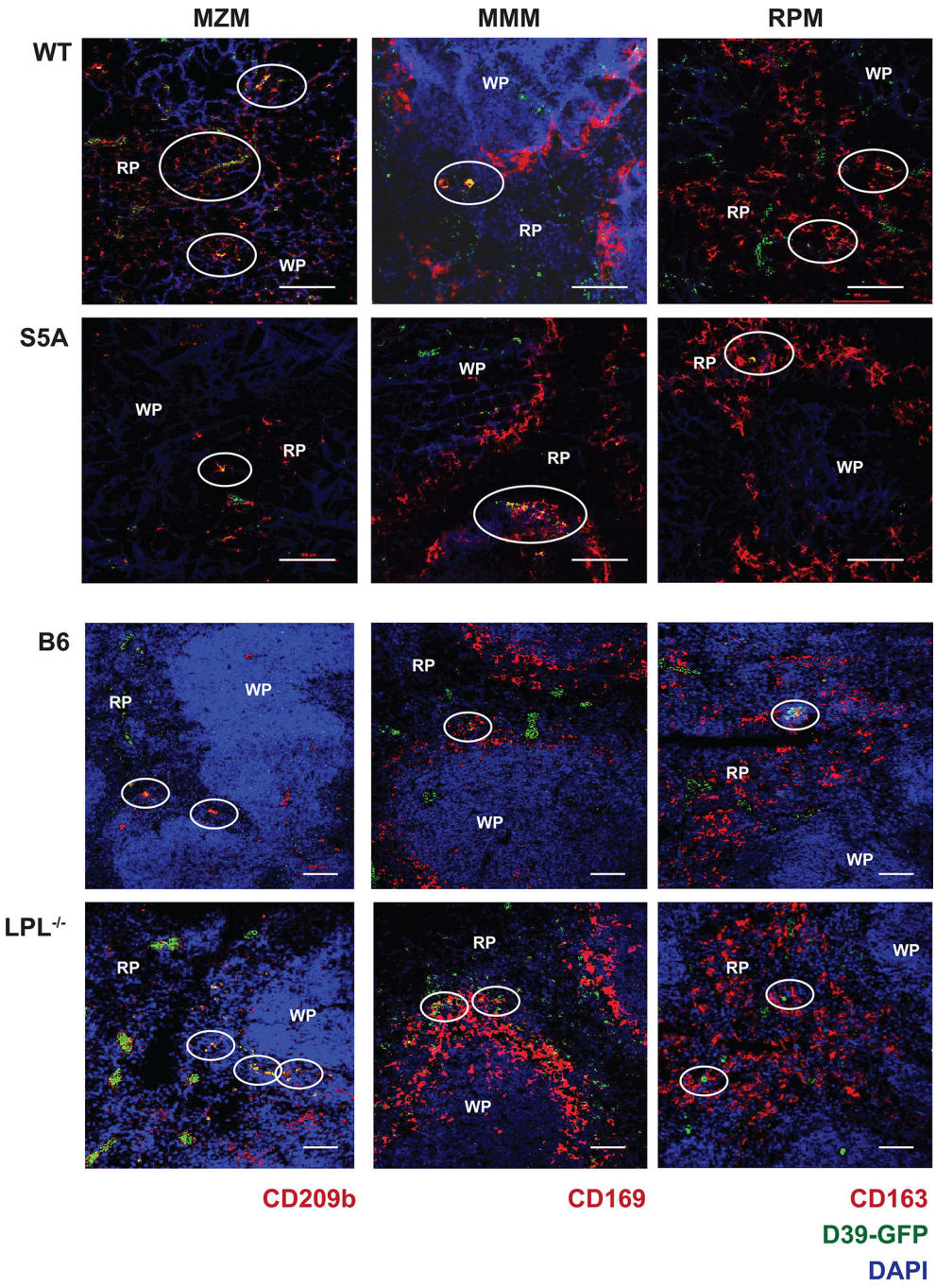

Figure 6. Reduction of MZM capture of pneumococci in S5A mice.

Frozen sections from spleens of WT, S5A, B6 and LPL$^{-/-}$ mice challenged with GFP-labeled pneumococci (D39-GFP) were stained with lineage-specific markers (red) and DAPI (blue) to illuminate lymphoid follicles. Areas of co-localization of pneumococci (green) and splenic macrophages are encircled. Scale bar indicates 100 μm. RP = red pulp. WP = white pulp.

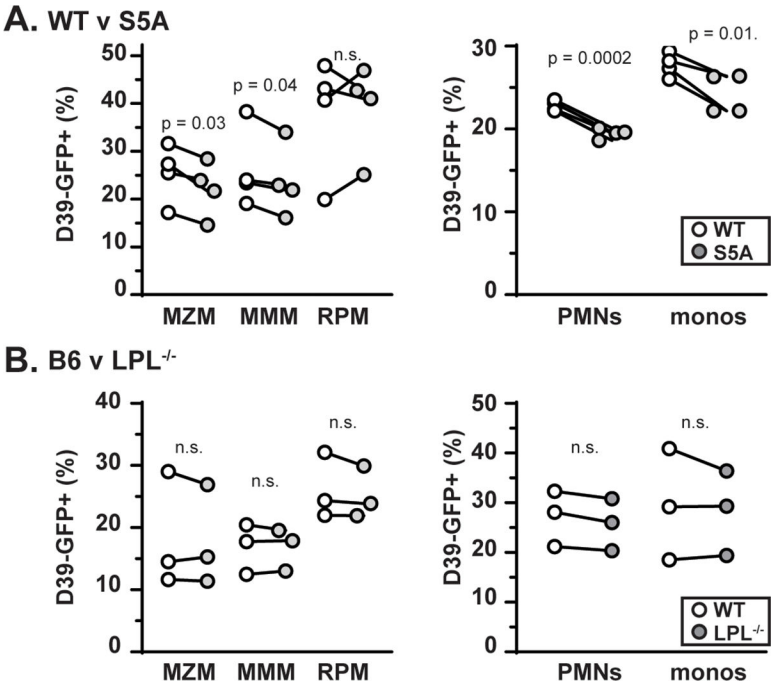

Figure 7. Impaired bacterial uptake by multiple phagocytic lineages derived from S5A mice.

A. Quantification of percentage of indicated cell type labeled with D39-GFP following challenge with pneumococcus *(i.v.)* in WT (open circle) or S5A (gray circle) mice. Four independent experiments were performed. **B.** Quantification of percentage of indicated cell type labeled with D39-GFP following challenge with pneumococcus (*i.v.*) in B6 (open circle) or $LPL^{-/-}$ (gray circle) mice. Three independent experiments were performed. (A, B) Each symbol represents the average value of two mice of each genotype included in each experiment. Paired results are indicated by lines connecting symbols. Wilcoxon paired signed rank test was used to test for significant differences. PMNs = polymorphonuclear cells, monos = monocytes.